ARTICLE

Efficient photocatalytic degradation of Acid Red 57 using synthesized ZnO nanowires

Hala A. Kiwaan[1] | Tarek M. Atwee[2] | Eslam A. Azab[1] | Ashraf A. El-Bindary[1]

[1]Chemistry Department, Faculty of Science, Damietta University, Damietta, Egypt

[2]Physics Department, Faculty of Science, Damietta University, Damietta, Egypt

Correspondence
Ashraf A. El-Bindary, Chemistry Department, Faculty of Science, Damietta University, Damietta 34517, Egypt.
Email: abindary@yahoo.com

Zinc oxide photocatalyst was synthesized through a low-temperature co-precipitation process using zinc sulfate as precursor for the degradation of Acid Red 57 (AR57) under UV irradiation. The activities of the prepared photocatalyst at different calcination temperatures (400, 500, and 600 °C) were investigated. The synthesized zinc oxides were characterized by different techniques such as X-ray diffraction, scanning electron microscopy, energy-dispersive X-ray spectroscopy, N_2 adsorption–desorption, and pH titration for the determination of the zero-point charge (pH_{ZPC}). The efficiency of photocatalytic degradation of ZnO prepared at the calcination temperatures of 400, 500, and 600 °C was 90.03, 77.67, and 72.71%, respectively, after 190 min. The kinetics and scavengers of the reactive species during the degradation were also investigated. It was found that the degradation of AR57 fitted first-order kinetics and the OH$^\bullet$ radicals were the main species. During irradiation, the formation of OH$^\bullet$ free radicals was ascertained by photoluminescence studies using terephthalic acid as the probe molecule.

KEYWORDS
Acid Red 57, fluorescence, kinetics, photocatalyst, ZnO nanowires

1 | INTRODUCTION

Organic dyes constitute an important source of environmental contamination, since they are toxic and mostly nonbiodegradable.[1] Conventional treatment methods such as biodegradation, adsorption, flocculation–coagulation, electrocoagulation, and conventional chemical oxidation are not effective enough in achieving total removal of these organic dyes from wastewaters.[2] Therefore, different advanced oxidation processes have been employed in the industry in the last decades in order to improve the oxidation of recalcitrant pollutants through the generation of highly reactive hydroxyl radicals (OH$^\bullet$).[3–5] Heterogeneous semiconductor photocatalysis has recently emerged as a promising technology, allowing the total mineralization of different refractory organic compounds in presence of either natural or artificial light.

Zinc oxide (ZnO) is one of the most commonly used materials for photocatalytic applications owing to its high chemical stability, low cost, low toxicity, and excellent oxidation properties.[6] As a well-known photocatalyst, ZnO possesses a wide bandgap of 3.37 eV and a large exciton binding energy (60 meV). Nevertheless, its low photocatalytic efficiency has been a major obstacle for its use in the degradation of pollutants on a large scale.[7] The semiconducting properties make this oxide a catalyst for the degradation of several recalcitrant substances by employing heterogeneous photocatalysis.[8,9] When this semiconductor absorbs ultraviolet or visible radiation, it encourages the formation of highly oxidizing species that destroy chemicals such as organic pollutants.[10] These parameters depend on the method of preparation of ZnO, which can be formed in several morphologies and sizes, especially in nanoscale dimensions.[11] Although the use of tiny ZnO particles with

large surface area can improve their photoactivity, nanoparticles of ZnO are better at the end of the process.[12,13]

In this work, we used a co-precipitation technique to synthesize ZnO nanowires by simple thermal annealing at different calcination temperatures (400, 500, and 600 °C). Systematic characterization of the as-prepared photocatalyst was carried out using various techniques. The photocatalytic activity was optimized, and a possible mechanism was proposed to explain the role of the ZnO nanowires under UV irradiation. The obtained results could be significant for the application of ZnO as a photocatalyst to remove AR57.

2 | RESULTS AND DISCUSSION

2.1 | Fourier transform infrared (FTIR) analysis

A broad peak observed at 3,387 cm^{-1} corresponds to the vibrational modes of the O–H bond (Figure 1).[14] A relatively less intense peak at 1,635 cm^{-1} represents the O–H stretching of the adsorbed water molecules. A very weak peak at ~2,303 cm^{-1} is recognized as due to the symmetric C–H bond, which may be present because of the environmental conditions. The vibrations of ZnO are in the range 400–600 cm^{-1}. The band at 500 cm^{-1} is connected with oxygen deficiency and/or oxygen vacancy deficiency present in ZnO.[15]

2.2 | X-ray diffraction (XRD)

The XRD patterns of the as-arranged ZnO nanowires at different thermal treatment temperatures are shown in Figure 2. The observed diffraction peaks connected with well-crystallized ZnO indicate the formation of the hexagonal wurtzite structure with lattice constants $a = b = 3.249$ Å and $c = 5.206$ Å (space group $P63mc$, JCPDS card no. 36–1,451).[16] No additional peaks due to impurities were detected, indicating the high purity of the as-prepared ZnO. It can be seen that the XRD patterns of the ZnO samples are similar at different annealing temperatures (Figure 2). The peaks at $2\theta = 31.78, 34.43, 36.27, 47.55, 56.62, 62.88, 67.97,$ and $69.11°$ can be attributed to the (100), (002), (101), (102), (110), (103), (112), and (201) planes of ZnO, respectively.[17] The crystallite size (D, Å) of
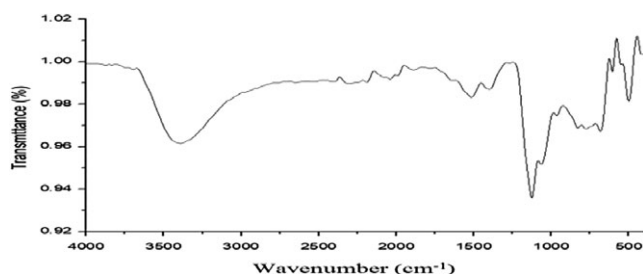

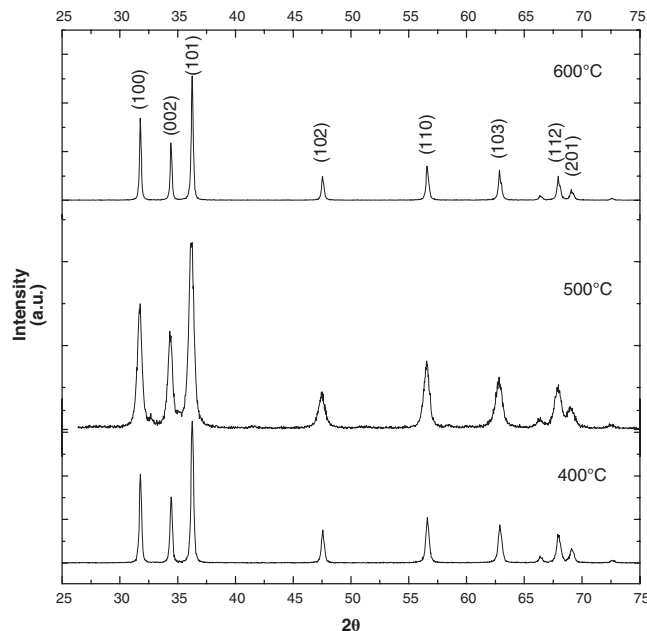**FIGURE 1** FTIR spectrum of ZnO at 400 °C

FIGURE 2 X-ray diffraction spectra of ZnO nanowires at different annealing temperatures (400, 500, and 600 °C)

the ZnO nanoparticles was calculated by using the Scherrer formula (Equation (1))[18]

$$\mathcal{D} = K\lambda/\beta \cos \theta B \tag{1}$$

where λ is the X-ray wavelength (1.54 Å), β is the angular width of the peak at half its maximum intensity (full width at half-maximum) corrected for instrumental broadening, $_B$ is the maximum of the Bragg diffraction peak, and K is the Scherrer constant (0.9 Å). The crystallite size of ZnO calculated from the high-intensity (101) peak was 40.5, 42.7, and 43.5 nm at the annealing temperatures 400, 500, and 600 °C, respectively. It can be easily concluded that by increasing the annealing temperature, the average grain size increases[19] and the specific surface area decreases.[10,20] These results can be explained on the basis of the increased extent of agglomeration of the ZnO particles.

2.3 | Scanning electron microscopy (SEM) analysis

Further morphological and structural characterization of ZnO nanowires was carried out through SEM analysis. Figure 3 shows the SEM images of the ZnO nanowires prepared by the co-precipitation technique at the calcination temperature of 400 °C. The SEM analysis indicates that the ZnO nanowires are formed with a diameter of ~40 nm and an average length of 296 nm. By increasing the calcination temperature, the nanowires grew longer.[21,22] The increase in the particle size is reflected in the decrease in the value of the bandgap (E_g). These data are more accurate than those obtained from the Scherrer formula, which usually carries out the evaluation from the sizes.
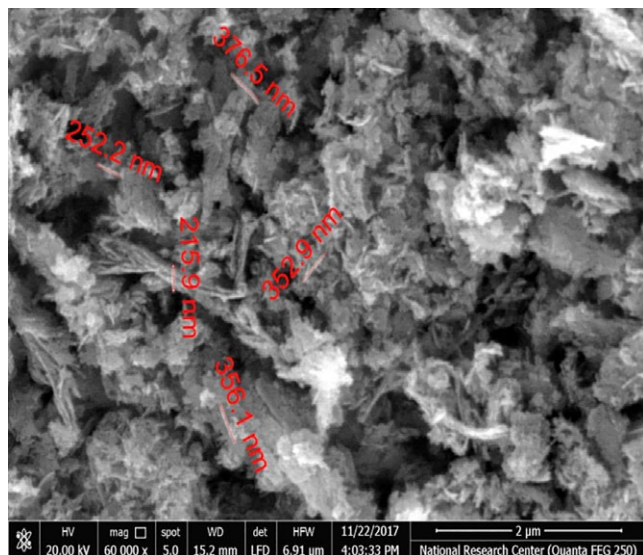
FIGURE 3 SEM image of ZnO nanowires at the calcination temperature of 400 °C

2.4 | Energy-dispersive X-ray spectroscopy (EDX)

The elemental composition of the synthesized ZnO nanowires was determined by EDX analysis coupled with SEM. The peaks assigned to Zn and O were seen, but no impurity peaks were detected, which further established that the synthesized ZnO was pure and consisted of only Zn and O (Figure 4). The weight and atomic percentage of Zn and O are 81.85 and 18.15%, and 51.15 and 48.85%, respectively.[23] The atomic percentages of Zn and O were found to be in the stoichiometric ratio 1:1. Similar results have been reported elsewhere for ZnO .[24,25]

2.5 | Brunauer–Emmett–teller (BET) surface area

The BET[26] surface area and Barrett–Joyner–Halenda (BJH) pore size of ZnO at 400 °C were investigated using N_2 adsorption/desorption measurements at 77 K (Figure 5). The N_2 adsorption–desorption isotherm of ZnO nanoparticles can be classified as type II, which refers to a nonporous solid at $P/P_o = 0.991$. The isotherm is completely reversible without any hysteresis loop, showing the absence of any pore type that permits capillary condensation process. The specific surface area of ZnO = 60 m^2/g calculated by BET equation in its normal range of applicability, adopting a
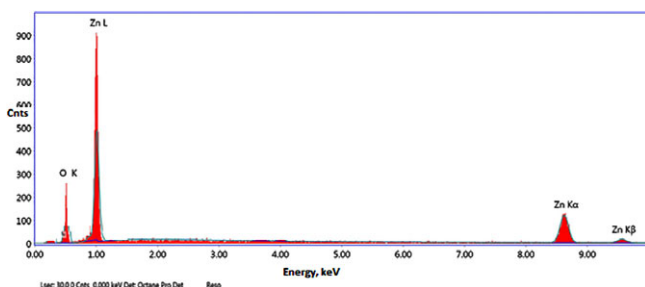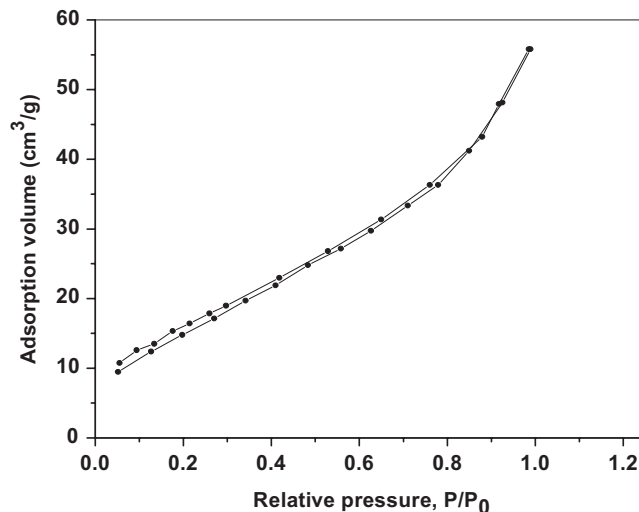

FIGURE 4 EDX spectrum of ZnO calcined at 400 °C

FIGURE 5 N_2 adsorption/desorption isotherm curve of ZnO calcined at 400 °C at 77 K

value of 16.2 Å for the cross-sectional area of the N_2 molecule. However, the total pore volume taken at a saturation pressure and expressed as liquid volume is 0.066 cm^3/g, and the pore radius calculated by BJH pore size distribution curve is equal to 19.22 Å. These results confirm the successful preparation of high-surface-area ZnO nanoparticles compared to the reference ZnO that had an area of ~13 m^2/g.[27]

2.6 | Determination of point of zero charge (pH_{PZC})

The pH value is one of the most important parameters for the degradation of AR57, as it determines which ionic species is near in the adsorbate solution and the surface charge of the sorbent. The surface charge of the ZnO was determined by PZC, which is defined as the pH (pH_{PZC}) at which the positive charges on the surface equal the negative charges.[28] The pH_{PZC} of ZnO was found to be 7.3 (Figure 6). This demonstrates that below this pH the ZnO acquires a positive charge owing to the protonation of functional groups and above this pH the surface of ZnO has a negative charge.

2.7 | Effect of operating parameters on the photocatalytic degradation of AR57

2.7.1 | Effect of calcination temperature

The activities of the prepared photocatalyst (ZnO) at different calcination temperatures (400, 500, and 600 °C) were investigated (Figure 7). The degradation efficiency of ZnO photocatalyst was found to be 90.03, 77.67, and 72.71% at the calcination temperatures of 400, 500, and 600 °C, respectively. The degradation efficiency of the ZnO samples was found to follow the order 400 °C > 500 °C > 600 °C after UV irradiation for 30 min, which could be associated with the grain size of the photocatalyst. The optimum temperature for synthesizing most efficient ZnO nanowires is
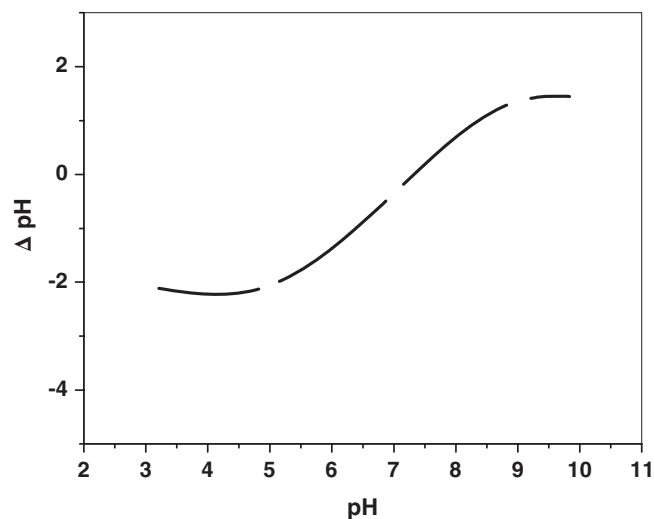
FIGURE 6 Relation between the initial pH and ΔpH of ZnO calcined at 400 °C

FIGURE 8 Effect of initial dye concentration on the photodegradation activity of ZnO calcined at 400 °C (20 min of irradiation time (lamp A), 2.5 g/L ZnO, and pH = 7)

400 °C and not below it. The precursor was not able to decompose into ZnO after calcination at 300 °C.

2.7.2 | Effect of initial dye concentration

The effect of initial dye concentration on its degradation was studied by varying the concentration of the dye from 10 to 100 mg/L, keeping the ZnO photocatalyst concentration at 2.5 g/L (Figure 8). It is found that the degradation efficiency of ZnO sample increased initially for a dye concentration up to 40 mg/L, and then it decreased. Therefore, the removal efficiency of the dye can be improved by a lower initial concentration of the dye.[29] This may be because more dye molecules were adsorbed on the surface of the photocatalyst when the initial concentration of the dye was high. Because many active sites were covered by the dye molecules, the adsorption of O_2 and OH^- on the photocatalyst decreased, leading to a reduction in degeneration of the radicals.[30] Furthermore, the photons were prevented from reaching the photocatalyst surface; hence, the adsorption of photons by the photocatalyst decreased.
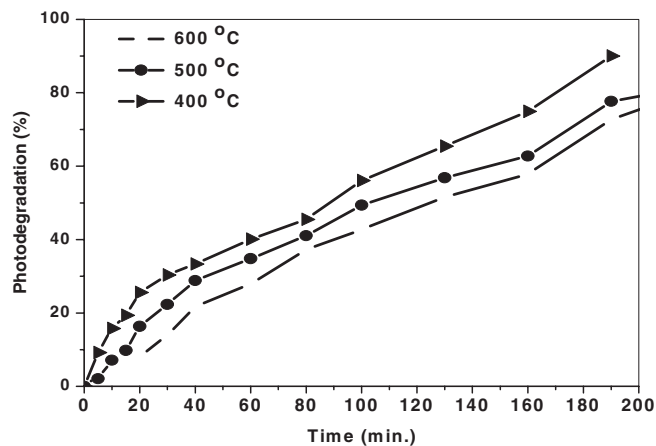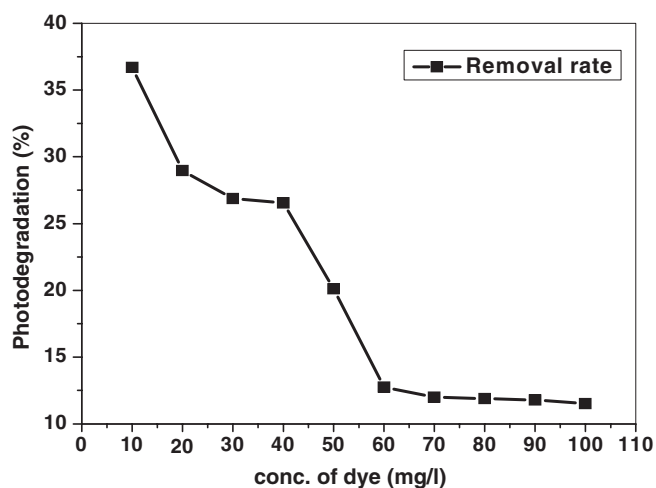
2.7.3 | Effect of ZnO concentration

Adequate concentration of the photocatalyst increases the generation rate of electron–hole pairs and thus the formation of $OH^\bullet$ radicals for increased photodegradation efficiency. Figure 9 shows the effect of ZnO concentration prepared at 400 °C (20 min irradiation time, 30 mg/L initial concentration of solution, and pH = 7). When the amount of photocatalyst was increased, more and more active sites were found on the photocatalyst surface, leading to enhanced formation of hydroxyl radicals.[31] Further increase in the amount of the photocatalyst had a negative effect because aggregation of the catalyst particles has a screening effect, which can prevent the photons from reaching the photocatalyst surface.[32,33]

2.7.4 | Effect of pH

The photocatalytic activity is strongly affected by the surface charge properties of the material, the charge of the molecule, the adsorption of the organic molecule on the photocatalyst surface, and the concentration of hydroxyl radicals.[34,35] The effect of varying pH from 2 to 10 in the initial AR57 solution is shown in Figure 10 for an initial AR57 concentration of 30 mg/L over ZnO (2.5 g/L and under UV irradiation (Lamp A). Decolorization efficiency decreases with increase in pH, showing that the pH of the dye solution determines the adsorption of the organic compound on the surface of ZnO and represents an important reaction step in the overall mechanism of dye oxidation.[36]

Dye degradation seems to be optimal at a pH around the zero-point charge pH (pHzpc), which is 7.3 for ZnO. At a pH lower than 7.3, the surface of ZnO photocatalyst is positively charged, whereas at a pH higher than 7.3 it becomes negatively charged. Since AR57 is an anionic dye, a pH lower than that corresponding to the zero-point charge favors the adsorption of AR57 molecule on the catalyst surface, which means improved degradation of AR57 under neutral
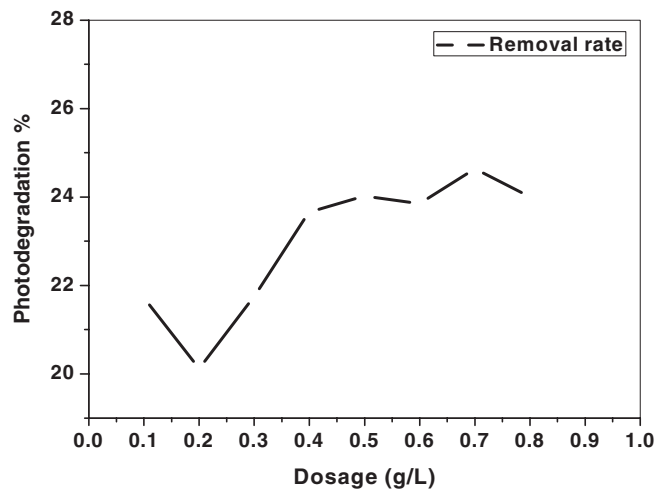

FIGURE 7 Effect of calcination temperature on the properties of ZnO (30 mg/L initial dye concentration, 2.5 g/L ZnO, and pH = 7)

FIGURE 9 Effect of concentration of ZnO prepared at 400 °C on the photodegradation activity of AR57 (20 min irradiation time (lamp A), 30 mg/L initial dye concentration, and pH = 7)

and acidic conditions. However, the increase in pH leads to an increase in Coulombic repulsion between the negatively charged ZnO surface and the OH⁻ species involved in the photocatalytic oxidation mechanism,[37] which will decrease the degradation efficiency.

2.7.5 | Effect of UV light intensity

Semiconductor photocatalyst absorbs light with an energy equal to or higher than bandgap energy,[38] which corresponds to the movement of electrons from the valence band to conduction band by separation of holes in the valance band. The rate of the photocatalytic degradation increases with increasing intensity of radiation. The chance of excitation of the photocatalyst can be enhanced by raising the intensity of the incident radiation.[39] But recombination of
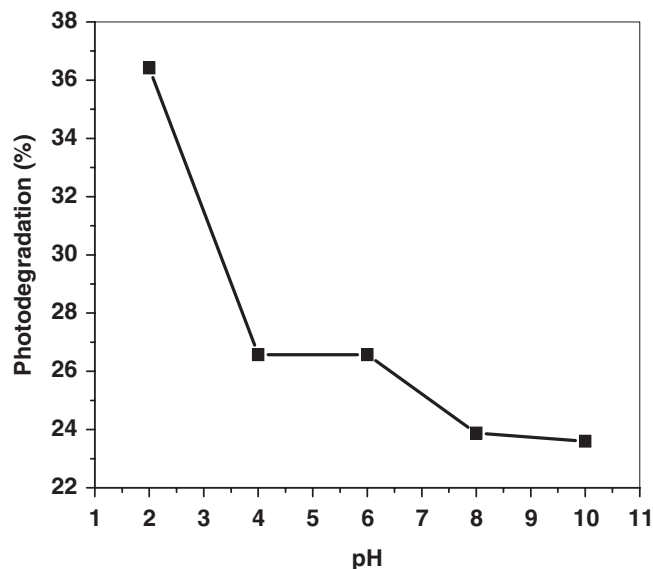
the electron–hole pair is a normally faced difficulty in photocatalysis. At lower light intensities, the electron–hole pair separation competes with recombination, which decreases the formation of free radicals and reduces the degradation of the organic molecules.[40] Therefore, enhancement of the photodegradation rate can be achieved by increasing the intensity of the incident radiation.[41] Dependence of the photocatalytic activity on the light intensity is shown in Figure 11.

2.8 | Estimation of chemical oxygen demand (COD)

COD is widely used as an effective parameter to measure the organic strength of wastewater.[42,43] The test allows the measurement of waste in terms of the total quantity of oxygen required for the oxidation of organic molecules to CO_2 and H_2O. The COD of the decolorization of AR57 dye solution was estimated at 0, 60, 120, and 180 min and found to be 145, 63, 55, and 35 ppm, respectively, using the $K_2Cr_2O_7$ oxidation method.[44] The photodecolorization efficiency was calculated using Equation (2) and found to be 56.5, 62.0, and 75.8% at projected times of 60, 120, and 180 min, respectively.

$$\text{Decolorization}\% = (\text{COD}_I - \text{COD}_F/\text{COD}_I) \times 100 \qquad (2)$$

where (COD_I) and (COD_F) are the COD values of blank and treated dye solutions, respectively.

2.9 | Degradation kinetics

The degradation rate of AR57 dye on ZnO at 400 °C (2.5 g/L) was estimated under UV irradiation (Figure 12). The degradation rate (D) of the dye was calculated using Equation (3):

$$D\% = (A_0 - A_t/A_0) \times 100, \qquad (3)$$

where A_0 represents the initial absorbance of AR57 solution (blank), and A_t its absorbance after time t (min) of

FIGURE 10 Effect of pH on the properties of ZnO calcined at 400 °C (20 min irradiation time (lamp A), 30 mg/L initial dye concentration, and 2.5 g/L ZnO)
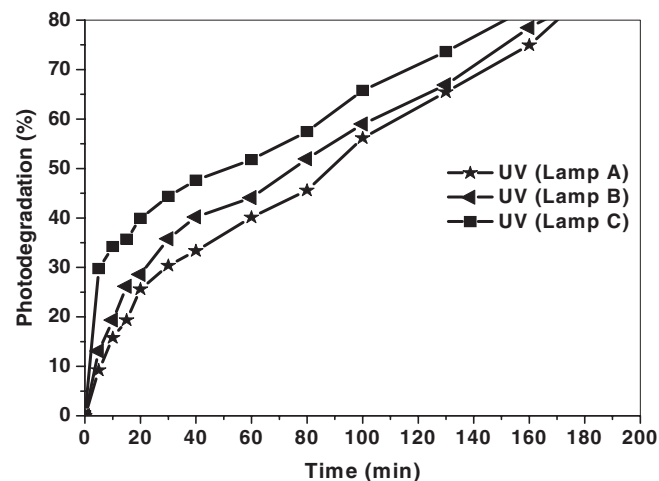

FIGURE 11 Effect of light intensity on the properties of ZnO calcined at 400 °C (30 mg/L initial dye concentration, 2.5 g/L ZnO, and pH = 7)
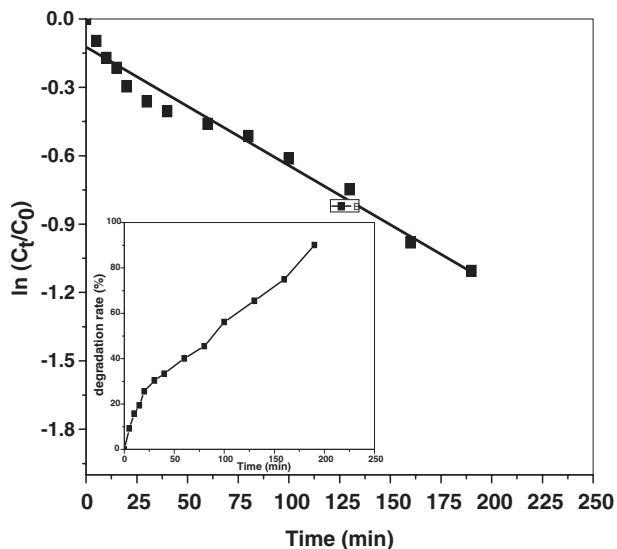
FIGURE 12 Photodegradation kinetic curve for photocatalytic degradation of AR57 over ZnO calcined at 400 °C under UV irradiation (lamp A) (30 mg/L initial dye concentration, 0.25 g/L ZnO, and pH = 7)

irradiation/reaction. According to the Beer–Lambert law, A_0 and A_t are proportional to C_0 and C_t, where C_0 and C_t are the concentration of the blank and sample at (t) time.

A pseudo-first-order kinetics model was tested to determine the kinetic rate constant (k) for the degradation process of AR57 on the ZnO nanoparticles, which is commonly expressed using Equation (4).

$$\ln (C_t/C_0) = kt. \tag{4}$$

The photodegradation rate constant (k, min^{-1}) was calculated from the slope of the straight line segment of the plot of $\ln(C_t/C_0)$ versus t as a function of the used experimental parameters. The linear fit between $\ln(C_t/C_0)$ and the reaction time t of AR57 dye follows a pseudo-first-order kinetic
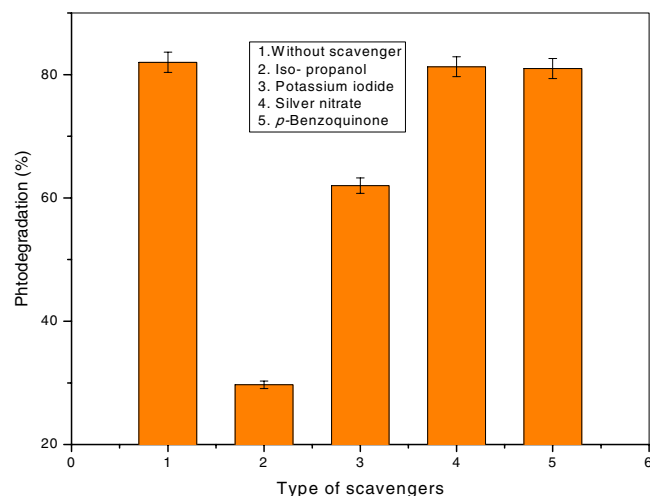

FIGURE 13 Photodegradation ratio of AR57 over ZnO calcined at 400 °C in the absence and presence of various scavengers (silver nitrate, potassium iodide, isopropanol, and p-benzoquinone) under UV irradiation (lamp A) (30 mg/L initial concentration of solution, 0.25 g/L ZnO, and pH = 7)

behavior (Figure 12)[13,27] with the correlation coefficient $R^2 = 0.989$, and the rate constant is 0.005 min^{-1}.

2.10 | Adsorption isotherms

Adsorption on a uniform surface with equivalent adsorption capacity is well described by the Langmuir isotherm, which suggests monolayer adsorption.[45] It also suggests no additional adsorption if dye molecules cover the active sites on the adsorbent. The Langmuir adsorption isotherm was used (Equation (5)):

$$C_e/C_{ads} = 1/Qb + 1/Q\,C_e, \tag{5}$$

where the concentration of the AR57 in the solution after equilibrium is C_e (mol/L), and the amount of AR57 retained on the ZnO is C_{ads} (mol/g). The maximum adsorption capacity of the monolayer is Q, and the apparent adsorption equilibrium constant is b. The values of Q and b are 2.74×10^{-5} mol/g and 1.059×10^4 L/mol. The separation value (R_L) is given by $1/(1 + bC_0)$, where C_0 is the initial concentration (0.0066), which indicates that the adsorption is favorable.[46]

2.11 | Stability of Photocatalyst ZnO

In addition to its photocatalytic property, the stability of photocatalyst is important in large-scale processes. Hence, to investigate the stability of the ZnO photocatalyst, recycling experiments of ZnO for the photocatalytic degradation of AR57 under UV irradiation were carried out. The photocatalyst was collected after each cycle by centrifugation, then washed with distilled water and ethanol, and dehydrated in an oven at 100 °C. The efficiency of the degradation of AR57 reduced from 90 to 85% after three cycles.

2.12 | Mechanism of Photodegradation

The photocatalytic reaction generally contains photoexcitation, charge separation and migration, and surface oxidation–reduction reactions.[47] The reactive species generated during illumination of photocatalysts are h$^+$, OH$^-$, and O$_2^{\bullet-}$. To understand the mechanism of ZnO for the degradation of AR57 dye, it is necessary to identify which reactive species plays a major role in the photocatalytic degradation process. During the photodegradation of dyes over ZnO, e$^-$, h$^+$, $^{\bullet}$OH, and O$_2^{\bullet-}$ are reduced by adding silver nitrate (e$^-$ scavenger), potassium iodide (h$^+$ scavenger), isopropanol ($^{\bullet}$OH scavenger), and p-benzoquinone (O$_2^{\bullet-}$ scavenger) into the reaction solution, respectively.[23] Figure 13 shows the degradation rate in the presence and absence of the scavengers. The addition of silver nitrate and p-benzoquinone caused slight change in the photocatalytic degradation of AR57 dye. However, the photodegradation percentage of AR57 was considerably reduced from 82 to 29.69% and 62% with the addition of isopropanol (OH$^{\bullet}$

scavenger) and potassium iodide (h^+ scavenger), respectively.[48] Hence, the hydroxyl radical ($OH^{\bullet}$) is the main reactive species during the photocatalytic degradation of AR57.

When the photocatalyst (ZnO) is illuminated with photons (h) of energy equal to or more than the bandgap energy of ZnO (3.37 eV), the electrons (e^-) are excited from the valence band (VB) to the conduction band (CB) with the simultaneous creation of holes (h^+) in the valence band:

$$ZnO + h \rightarrow ZnO\left(h^+_{[VB]}\right) + ZnO\left(e^-_{[CB]}\right), \quad (6)$$
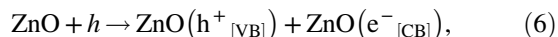
where h is the energy required to transfer the electron from VB to CB. The electrons generated through irradiation could be readily surrounded by the O_2 absorbed on the photocatalyst surface or the dissolved O_2[49] to give superoxide radicals ($O_2^{\bullet-}$):

$$e^-_{(CB)} + O_2 \rightarrow O_2^{\bullet-} \quad (7)$$
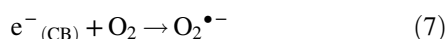
Subsequently, $O_2^{\bullet-}$ can react with H_2O to produce the hydroperoxy radical ($HO_2^{\bullet}$) and hydroxyl radical ($OH^{\bullet}$), which are strong oxidizing agents to decompose the organic molecule:

$$O_2^{\bullet-} + H_2O \rightarrow HO_2^{\bullet} + OH^{\bullet} \quad (8)$$
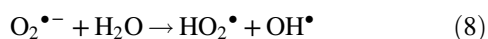
Simultaneously, the photo-induced holes could be trapped by surface hydroxyl groups (or H_2O) on the photocatalyst surface to give hydroxyl radicals ($OH^{\bullet}$).[30]

$$OH^- + h^+_{(VB)} \rightarrow OH^{\bullet}_{ad}.$$

$$H_2O \leftrightarrow (H^+ + OH^-) + h^+_{(VB)} \rightarrow OH^{\bullet} + H^+. \quad (9)$$
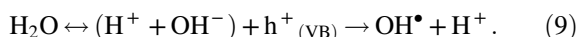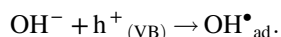
Finally, the organic molecules (AR57) will be oxidized to yield carbon dioxide and water as follows:

$$OH^{\bullet} + AR57 + O_2 \rightarrow products\,(CO_2\,and\,H_2O) \quad (10)$$
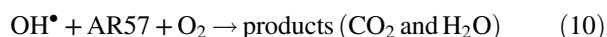
Meanwhile, the recombination of the positive hole and electron can happen, which can reduce the photocatalytic activity of prepared photocatalyst (ZnO):

$$ZnO\left(h^+_{(VB)}\right) + ZnO\left(e^-_{(CB)}\right) \rightarrow ZnO. \quad (11)$$
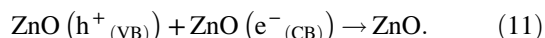
The formation of $OH^{\bullet}$ free radicals is determined by means of photoluminescence studies using terephthalic acid (TPA) as a probe molecule. TPA is known to react with $OH^{\bullet}$ free radicals to yield 2-hydroxyterphthalic acid, which shows a characteristic luminescence peak at 420 nm.[50] The intense luminescence peak at 420 nm for the sample containing ZnO + TPA after irradiation for 30, 60, 90, 120, and 180 min clearly shows the presence of $OH^{\bullet}$ free radicals during irradiation (Figure 14).

2.13 | Correlation analysis

It is important to study the correlation between the physical and chemical properties of the photocatalyst and its degradation properties. The degradation efficiency of ZnO
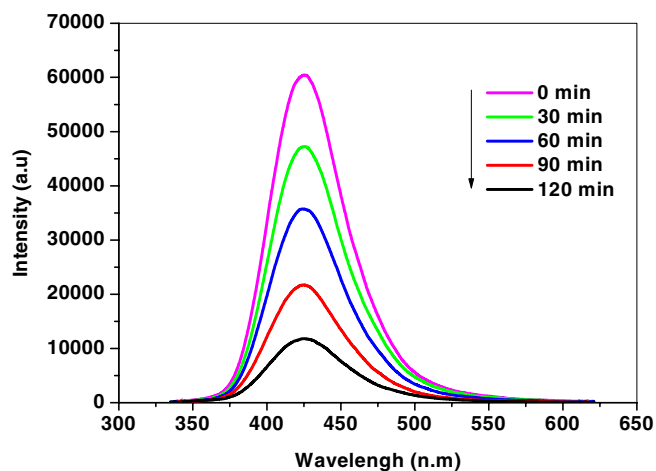

FIGURE 14 Photoluminescence spectra of ZnO + TPA after irradiation (30 mg/L initial dye concentration, 0.25 g/L ZnO, 5×10^{-5} M terephthalic acid, and pH = 7) with the excitation wavelength of 315 nm

photocatalyst was found to be 90.03, 77.67, and 72.71% at calcination temperatures 400, 500, and 600 °C, respectively. Figure 15 shows that the relation between the particle grain size of the photocatalyst at 400, 500, and 600 °C and the degradation efficiency. The particle grain size of ZnO at 400, 500, and 600 °C was found to be 40.5, 42.7, and 43.5 nm, respectively. As the grain size decreases, the specific surface area increases and the photocatalyst gives a high degradation rate of AR57. The best photocatalytic degradation of AR57 was observed over ZnO calcined at 400 °C.

3 | EXPERIMENTAL

3.1 | Materials

Zinc sulfate heptahydrate ($ZnSO_4 \cdot 7H_2O$) and oxalic acid dihydrate ($(COOH)_2 \cdot 2H_2O$) were supplied by Sigma-Aldrich and used as received. A commercial textile dye Acid Red 57 (Table 1) was obtained from Cromatos SRL, Italy, and was used without any further purification. A stock solution of AR57 (1.0 g/L) was used, which could be diluted to the required concentration with deionized water in the experiment. All chemical reagents were of analytical grade and used without any further purification. Samples were then conserved in desiccators over anhydrous $CaCl_2$ for further use.

3.2 | Photocatalyst synthesis

ZnO was synthesized through a low-temperature co-precipitation process using deionized water as solvent. Aqueous ammonia (25%, 100 mL) was added dropwise to zinc sulfate heptahydrate (0.5 mol, 143.77 g) dissolved in deionized water. The solution was heated at 60 °C under continuous agitation using a magnetic stirrer for 30 min. During stirring, a solution of sodium bicarbonate (0.3 mol, 25.2 g) as reducing
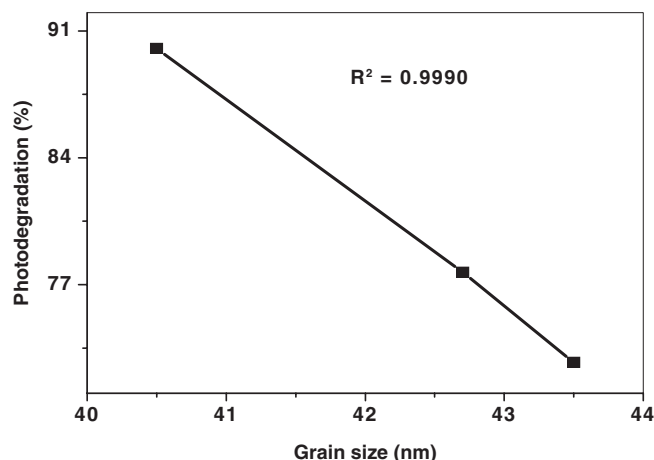
FIGURE 15 Correlation curve between XRD grain size of ZnO calcined at 400, 500, and 600 °C and the photodegradation efficiency of AR57
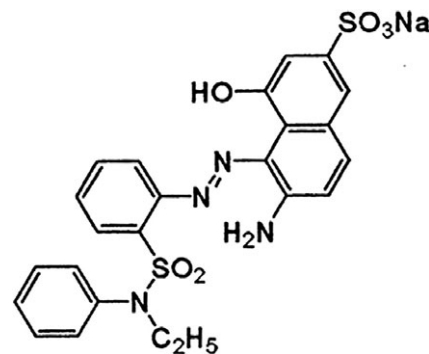
agent was added. The white precipitate of $Zn(OH)_2$ was filtered, washed several times by deionized water, and dried at 100 °C for 5 hr. Finally, ZnO was obtained by thermal treatment at different calcination temperatures of 400, 500, and 600 °C for 5 hr. Moreover, the dried ZnO samples were sieved with a 200-μm mesh in order to obtain small, uniform particles.

3.3 | Photocatalyst characterization

FT-IR analysis was carried out using a JASCO-FT/IR-4100 spectrometer (Jasco, Easton, MD). Finely ground samples were incorporated into KBr disks prior to analysis in the wavenumber range 400–4,000 cm^{-1}. The surface morphology of the samples was examined using SEM analysis at the accelerating voltage of 20 kV (JEOL-JSM-6510 LV). The elemental distribution of ZnO was analyzed using EDX on a Leo1430VP microscope with operating voltage 5 kV. Structural variations of the as-prepared materials were investigated by XRD using a Shimadzu XRD-6000 diffractometer

(Shimadzu Corporation, Tokyo, Japan) equipped with Cu Kα radiation ($\lambda = 1.54$ Å). The 2θ value was varied between 5 and 80° at the scanning rate of 0.02°/min. The crystal system, space group, and lattice parameters were considered and optimized using CRYSFIRE and CHEKCELL computer programs.[51] A UV–visible spectrophotometer (Perkin-Elmer AA800 Model AAS) was employed for absorbance measurements of the samples using a 1.0-cm quartz cell. A fluorescence spectrometer (LUMINA, Thermo Scientific) was used for fluorescence measurements of the samples using a 1.0-cm quartz cell. The adsorption/desorption isotherm of N_2 on ZnO at 77 K was evaluated with a Quantachrome Touch Win Instruments version 1.11. For the analysis of the curves, we utilized the BET method (P/P_o from 0.05 to 0.35) for specific area, t-plot method for external area, volume, and area of micropores; and the BJH method for diameter determination of the mesopores. A pH meter (HANNA instrument model 211) and water bath (Maxturdy 30 Wisd) were used for pH modification and shaking, respectively. A HANNA instrument wastewater behavior photometer (model HI 83214) was used for the measurement of COD.

3.4 | Determination of point of zero charge

The point of zero charge (pH_{PZC}) was resolved by the solid addition method.[52] A series of 0.1 M KNO_3 solutions (50 mL each) were prepared and their pH values (pH_0) were tuned in the range of 1.0–12.0 by the addition of 0.1 mol/L HCl and 0.1 mol/L NaOH. To each solution, 0.1 g of ZnO was added and the suspensions were disturbed using the shaking water bath at 25 °C. The final pH values of the supernatant were determined (pH_f) after 48 hr. The difference between initial (pH_0) and final (pH_f) values ($\Delta pH = pH_0 - pH_f$) (Y-axis) was plotted against the initial pH_0 (X-

TABLE 1 Properties of the adsorbate Acid Red 57 (AR57) used in the study

Type	Anionic (AR57)
Chemical formula	$C_{24}H_{21}N_4NaO_6S_2$
Molecular weight (g/mol)	548.57
Wavelength of maximum absorption (nm)	512
Molar extinction coefficient, ε_{512} (M^{-1} cm^{-1})	23,660
Chemical structure	

axis). The intersection of the resulting curve yielded the pH_{PZC} where $\Delta pH = 0$.

3.5 | Photocatalytic dye degradation experiments

The experiment was set up for the photodeclorization of 100 mL (30 mg/L, pH = 7.0) aqueous solution of AR57 containing 2.5 g/L of the photocatalyst. The solution was taken in a cylindrical Pyrex glass cell (5 cm inside diameter and 10 cm height) as the reactor. The suspensions were irradiated under atmospheric condition with a medium-pressure UV lamp (Philips) that was positioned above the reactor (distance 20 cm). The photocatalytic experiments were carried out under UV irradiation at room temperature using three UV lamps (A, B, and C) with E_{photon} (eV) 3.10–3.94, 3.94–4.43, and 4.43–12.4 with λ_{max} (nm) 400–315, 315–280, and 280–100, respectively. During the irradiation, the suspension was sampled at the regular time intervals. Before illumination, the dispersion was magnetically stirred for 30 min (in the dark) in order to ensure adsorption equilibrium between the photocatalyst surface and the AR57 dye. Thus, the effect of surface adsorption in the removal of AR57 was eliminated. The influence of the pH of the initial solution was evaluated at pH values from 2 to 10 (adjusted using HCl (0.1 M) and NaOH (0.1 M)), while AR57 dye concentration was preset at 30 mg/L for 2.5 g/L of ZnO photocatalyst. The photocatalyst dosage was varied from 0.1 to 0.8 g/L, for 30 mg/L of AR57 solution, at pH 7. The influence of the AR57 dye concentration was also evaluated by varying its concentration from 10 to 100 mg/L, at a fixed pH of 7, in the presence of 2.5 g/L of ZnO photocatalyst. Each sample was taken out at a given time interval and immediately centrifuged at 20,000 rpm for 10 min to remove any suspended solid catalyst particles, for analysis. Finally, the absorbance of AR57 in the supernatant liquid was recorded by a UV–visible spectrophotometer at the maximum adsorption wavelength of AR57, i.e., $\lambda_{max} = 512$ nm.

The degradation rate (D) of the dye was calculated using Equation (3). The photodegradation of the pollutants follows pseudo-first-order kinetics according to the Langmuir–Hinshelwood model, so the photodecolorization rate of each dye was studied using Equation (4). To confirm the photodegradation results, COD of the samples before and after photodegradation experiments was calculated at regular time intervals using the closed reflux titrimetric method.[53,54]

4 | CONCLUSIONS

Photocatalytic activity of ZnO photocatalyst was examined for the treatment of aqueous solutions containing AR57 under UV light irradiation. ZnO sample was synthetized by co-precipitation and calcined at different temperatures, and they were characterized by different spectroscopic techniques. Based on the XRD and SEM measurements, the ZnO was present in the hexagonal wurtzite phase, and the size of ZnO was 40.5, 42.7, and 43.5 nm at annealing temperatures 400, 500, and 600 °C, respectively. In fact, the highest photocatalytic AR57 removal from aqueous solution was achieved by using ZnO at 400 °C as photocatalyst, confirmed also by the evaluation of the kinetic constant for AR57 degradation. The effect of the operating parameters such as pH, catalyst dosage, and the initial dye concentration, as well as the influence of UV irradiation intensity, was estimated. It was found that the degradation of AR57 fitted first-order kinetics and $OH^\bullet$ radicals were the main species. Formation of $OH^\bullet$ free radicals during irradiation was ascertained by photoluminescence studies using terephthalic acid as the probe molecule. The degradation extent was checked by UV–vis spectroscopy and confirmed by COD.

ORCID

Ashraf A. El-Bindary http://orcid.org/0000-0002-4494-3436

REFERENCES

[1] J. E. B. McCallum, S. A. Madison, S. Alkan, R. L. Depinto, R. U. R. Wahl, *Environ. Sci. Technol.* **2000**, *34*, 5157.
[2] A. Hassani, L. Alidokht, A. R. Khataee, S. Karaca, *J. Taiwan Inst. Chem. Eng.* **2014**, *45*, 1597.
[3] H. B. Hadjltaief, P. DaCosta, M. E. Galvez, M. B. Zina, *Ind. Eng. Chem. Res.* **2013**, *52*, 16656.
[4] M. R. Hoffmann, S. T. Martin, W. Choi, D. W. Bahnemann, *Chem. Rev.* **1995**, *95*, 69.
[5] W. Wang, S. Li, C. Pan, S. Liu, T. Luo, G. Dai, *J. Chin. Chem. Soc.* **2018**, *65*, 252.
[6] C. G. Tian, Q. Zhang, A. P. Wu, M. J. Jiang, Z. L. Liang, B. J. Jiang, H. G. Fu, *Chem. Commun.* **2012**, *48*, 2858.
[7] A. Moezzi, A. M. McDonagh, M. B. Cortie, *Chem. Eng. J.* **2012**, *185*, 1.
[8] K. M. Lee, C. W. Lai, K. S. Ngai, J. C. Juan, *Water Res.* **2016**, *88*, 428.
[9] V. Oskoei, M. H. Dehghani, S. Nazmara, B. Heibati, M. Asif, I. Tyagi, S. Agarwal, V. K. Gupta, *J. Mol. Liq.* **2016**, *213*, 374.
[10] X. Chen, Z. Wu, Z. Gao, B.-C. Ye, *Nanomaterials* **2017**, *7*, 1.
[11] J. Fei, J. Li, *Adv. Mater.* **2015**, *27*, 314.
[12] A. Taheri Najafabadi, F. Taghipour, *J. Photochem. Photobiol. B Chem.* **2012**, *248*, 1.
[13] A. Pruna, Z. Wu, J. A. Zapien, Y. Y. Li, A. Ruotolo, *Appl. Surf. Sci.* **2018**, *441*, 936.
[14] A. R. Prasad, P. R. Ammal, A. Joseph, *Mater. Res. Bull.* **2018**, *102*, 116.
[15] G. Xiong, U. Pal, J. G. Serrano, K. B. Ucer, R. T. Williams, *Phys. Stat. Sol.* **2006**, *3*, 3577.
[16] K. Omri, I. Najeh, R. Dhahri, J. El Ghoul, L. El Mir, *Microelect. Eng.* **2014**, *128*, 53.
[17] R. Krithiga, G. Chandrasekaran, *J. Cryst. Growth* **2009**, *311*, 4610.
[18] A. L. Patterson, *Phys. Rev.* **1939**, *56*, 978.
[19] O. Mekasuwandumrong, P. Pawinrat, P. Praserthdam, J. Panpranot, *J. Chem. Eng.* **2010**, *164*, 77.
[20] K. Omri, I. Najeh, L. El Mir, *Ceram. Int.* **2016**, *42*, 8940.
[21] Y. L. Chen, L. C. Kuo, M. L. Tseng, H. M. Chen, C. K. Chen, H. J. Huang, *Opt. Express* **2013**, *21*, 7240.
[22] M. R. Khanlary, V. Vahedi, A. Reyhani, *Molecules* **2012**, *17*, 5021.
[23] X. Chen, Z. Wu, D. Liu, Z. Gao, *Nanoscale Res. Lett.* **2017**, *12*, 143.
[24] R. Kumar, G. Kumar, A. Umar, *Mater. Lett.* **2013**, *97*, 100.
[25] A. Sedky, T. A. El-Brolossy, S. B. Mohamed, *J. Phys. Chem. Solids* **2012**, *73*, 505.
[26] S. Brunauer, P. H. Emmett, E. Teller, *J. Am. Chem. Soc.* **1938**, *60*, 309.
[27] D. E. Wurster, E. Oh, J. C. Wang, *J. Pharm. Sci.* **1995**, *84*, 1301.

[28] S. Sadaf, H. N. Bhatti, M. Arif, M. Amin, F. Nazar, *Chem. Ecol.* **2015**, *31*, 252.

[29] Y. Ni, D. Jiang, Y. Gao, X. Zhu, H. Zhang, *Mater. Res. Bull.* **2018**, *99*, 37.

[30] L. Saikia, D. Bhuyana, M. Saikia, B. Malakar, D. K. Dutta, P. Sengupta, *Appl. Catal. A Gen.* **2015**, *490*, 42.

[31] H. Faghihian, A. Bahranifard, *Iran. J. Catal.* **2011**, *1*, 45.

[32] H. R. Pouretedal, A. Norozi, A. H. Keshavarz, A. Semnani, *J. Hazard. Mater.* **2009**, *162*, 674.

[33] A. Elaziouti, N. Laouedi, B. Bekka, *Environ. Sci. Poll. Res.* **2016**, *23*, 15862.

[34] X. Wang, Z. Wu, W. Yin, W. Wang, X. Wang, Y. Bu, J. Zhao, *J. Hazard. Mater.* **2013**, *262*, 16.

[35] A. Nezamzadeh-Ejhieh, E. Shahriari, *J. Ind. Eng. Chem.* **2014**, *20*, 2719.

[36] V. Kuzhalosai, B. Subash, A. Senthilraja, P. Dhatshanamurthi, M. Shanthi, *Spectrochim. Acta A* **2013**, *115*, 876.

[37] A. Jain, A. Asthma, K. Marazban, *J. Appl. Chem.* **2014**, *2*, 13.

[38] J.-L. Shie, C.-H. Lee, C.-S. Chiou, C.-T. Chang, C.-C. Chang, C.-Y. Chang, *J. Hazard. Mater.* **2008**, *155*, 164.

[39] T. A. Saleh, M. A. Gondal, Q. A. Drmosh, Z. H. Yamani, A. Al-Yamani, *Chem. Eng. J.* **2011**, *166*, 407.

[40] B. Neppolian, H. C. Choi, S. Sakthivel, B. Arabindoo, V. Murugesan, *J. Hazard. Mater.* **2002**, *89*, 303.

[41] A. Gnanaprakasam, V. M. Sivakumar, M. Thirumarimurugan, *Ind. J. Mater. Sci.* **2015**, *28*, 1.

[42] M. C. Hasegawa, J. F. Daniel, K. Takashima, G. A. Batista, S. M. da Silva, *Environ. Technol.* **2014**, *35*, 1589.

[43] M. Y. Ghalya, J. Y. Faraha, A. M. Fathy, *Desalination* **2007**, *217*, 74.

[44] J. Ziemianska, E. Adamek, A. Sobczak, I. Lipska, A. Makowski, W. Baran, *Probl. Miner. Process.* **2010**, *45*, 5.

[45] G. Crini, *Dyes Pigm.* **2008**, *77*, 415.

[46] F. C. Wu, R. L. Tseng, R. S. Juang, *Water Res.* **2001**, *35*, 613.

[47] E. Topkaya, M. Konyar, H. C. Yatmaz, K. Ozturk, *J. Coll. Interf. Sci.* **2014**, *430*, 6.

[48] N. Huang, J. X. Shu, Z. H. Wang, M. Chen, C. G. Ren, W. Zhang, *J. Alloys Comp.* **2015**, *648*, 919.

[49] A. Houas, H. Lachheb, M. Ksibi, *Appl. Catal. B: Environ.* **2001**, *31*, 145.

[50] T. N. Muthy, K. Deepti, A. M. Umabala, A. V. P. Rao, *Der Pharma Chem.* **2016**, *8*, 140.

[51] R. Shirley, *The CRYSFIRE System for Automatic Powder Indexing: User's Manual*, The Lattice Press, Guildford, UK **2002**.

[52] K. Z. Elwakeel, A. A. El-Bindary, E. Y. Kouta, E. Guibal, *Chem. Eng. J.* **2018**, *332*, 727.

[53] A. Nezamzadeh-Ejhieh, H. Zabihi-Mobarakeh, *J. Indust. Eng. Chem.* **2014**, *20*, 1421.

[54] H. Guan, X. Zhou, W. Wen, B. Jin, J. Li, S. Zhang, *J. Chin. Chem. Soc.* **2018**, *65*, 706.